Journal of Thermal Analysis and Calorimetry (2019) 136:471–481
https://doi.org/10.1007/s10973-018-7690-0

Thermoanalytical and dynamic mechanical analysis of commercial geomembranes used for fluid retention of leaching in sanitary landfills

Clever Aparecido Valentin[1] · Jefferson Lins da Silva[1] · Marcelo Kobelnik[2] · Clovis Augusto Ribeiro[3]

Received: 23 May 2018 / Accepted: 17 August 2018 / Published online: 23 August 2018

Abstract
Studying thermal behavior is very important for monitoring the quality of polymers on an industrial scale. Commercial geomembranes are materials with low permeability that can be used for multiple purposes, such as geotechnical engineering in liners for potable water. They can also be used as liners for waste liquid, e.g., sewage sludge and soil coverings for landfills. In this paper, the mechanical and thermal behavior of four geomembranes with thicknesses around 2.1, 1.9, 1.7 and 0.8 mm, sold in Brazil by different companies, was evaluated. Thickness, density, tension, puncture and tear resistance and carbon black content were used to characterize the properties of these materials. Thermogravimetry, differential thermal analysis, differential scanning calorimetry (DSC) and dynamical mechanical analysis (DMA) were used to examine the evolution of these geomembranes thermal behavior. Moreover, activation energy of the thermal decomposition was estimated from non-isothermal kinetics. The results obtained by thermogravimetry showed that the geomembranes have a different thermal behavior from each other. Data obtained by DSC showed a widening of the melting peak after the second heating. Activation energy values obtained by the Flynn–Wall–Ozawa and Capela–Ribeiro isoconversional methods for each sample showed variations between them. Based on the DMA experiment, the store modulus (E'), loss modulus (E'') and tan δ showed different behaviors for the 0.8-mm sample and no significant changes in the other samples. Concerning the mechanical properties, it can be observed that the density and black carbon data have compatible values between the samples.

Keywords Geomembranes · TG/DTG · DMA · Mechanical texts

Introduction

Final waste disposal is a public health problem in many parts of the world due to it being deposited in inappropriate places. In Brazil, the government passed a national solid waste law in 2010, which provides guidelines for these materials [1]. Impacts caused to the environment by some types of waste can cause irreversible damage to the environment. As an example, there are many problems related to alkaline batteries and cellular batteries, which contain toxic metals, such as mercury, lead, cadmium, among other materials [2, 3]. In addition, disposing of post-consumer polymer materials of various natures is problematic and causes serious damage to the environment [4]. Considering this situation, implementing controlled landfills requires using soil protection geomembranes for landfills, which avoid contamination with the soil. During installation, the geomembranes are welded between the parts at installation sites using intense heat, which is done using a thermofusion apparatus [5]. In addition, these geomembranes should be installed in soil with an adequate slope to direct the slurry generated by the deposited waste to an appropriate stabilization pond where it should be treated. In fact, the pond that receives the slurry must also have the base soil covered with a geomembrane to prevent liquid from leaching into the soil [6].

✉ Clever Aparecido Valentin
cclever@sc.usp.br

[1] São Carlos School of Engineering - EESC, University of São Paulo - USP, São Carlos, SP, Brazil

[2] Centro Universitário do Norte Paulista - UNORP, São José do Rio Preto, SP, Brazil

[3] Departamento de Química Analítica, Universidade Estadual Paulista - UNESP, Araraquara, SP, Brazil

The most common types of geomembranes are high-density polyethylene (HDPE), polyvinyl chloride (PVC) (plasticized), low-density polyethylene (LDPE), ethylene propylene diene terpolymer (EPDM), etc. [7–10]. In Brazil, HDPE is among the most used in water reservoirs for irrigation, soil impermeabilization, etc. [11, 12].

Due to the versatility of HDPE which can be used in different types of plastic materials, there is a large body of literature on various applications of this material in the most diverse areas of knowledge. For example, Rajeshwari [13] reported on the thermal decomposition and kinetics behavior of HDPE reinforced with various concentrations of carbon nanotubes. The values obtained from the kinetic evaluations of the four methods used presented a decrease in the activation energy values for the concentrations of 0.25–0.75 vol% of carbon nanotubes. The author also found that for the major concentration (> 0.75 vol%), the value of the activation energy had increased.

Recently, Khedri and Elyasi have studied the pyrolysis of HDPE in 400, 410, 420 and 430 °C using a differential scanning calorimetry (DSC) instrument in an isothermal condition. The obtained values of decomposition heat of HDPE of this study were 1375 ± 233 kJ kg^{-1}. The authors state that the obtained values are higher than those in the literature and attribute this to using the isothermal method, whereas the non-isothermal method was used by other authors [14].

Rowe and Ewais [15] studied five HDPE geomembranes with thicknesses of 0.5, 1.0, 1.5, 2.0 and 2.4 mm under immersion of these materials in leachate at various temperatures. The evaluation parameters of this study showed a decrease or increase in antioxidants/stabilizers under standard (Std-) and high-pressure (HP-) oxidative induction time (OIT) conditions. The results indicate that in both Std-OIT and HP-OIT, there was a reduction in the antioxidant/stabilizer with the increase in geomembrane thickness.

Aboulkas et al. carried out a thermoanalytical and kinetic study of HDPE, LDPE and polypropylene (PP) polymers found in recyclable materials. The values obtained for the activation energy under non-isothermal conditions for HDPE, using the Flynn–Wall–Ozawa method, ranged from 208 to 247 kJ mol^{-1} [16].

Therefore, in order to contribute to geomembrane research, the objective of this work was to evaluate the thermal, thermomechanical and mechanical resistances of a sample of commercial geomembranes used in Brazil to cover soil in sanitary landfills. Furthermore, the importance of these analyses is probably due to the difference in production of geomembranes by different companies, attributed to the different raw material proportions. In addition, this study also suggests using thermoanalytical techniques for geomembrane production control.

A thermoanalytical study was carried out with thermogravimetric (TG), differential thermal analysis (DTA), DSC and dynamic mechanical analysis (DMA). The evaluation of physical properties was: density (specific gravity method), thickness (20-kPa pressure) and carbon black content (using the muffle furnace technique). The mechanical properties such as the tensile test (dumbbell-shaped test specimens), tear resistance and puncture resistance (index puncture resistance) were also evaluated.

Experimental

Interest in evaluating these materials is aimed at knowing their physical limits, as commercial geomembrane coils (when purchased from a manufacturer) can be stored in unhealthy places before they are used, and therefore, knowledge about their thermal limits is important. Moreover, evaluating the physical resistance of these materials is important so that most appropriate materials are acquired for the type of landfill. Moreover, polymer research by thermogravimetry and calorimetry is an important source of information regarding the thermal behavior of these materials and is very useful for industrial processing of commercial membranes [17].

Geomembrane samples were obtained from commercial coils, manufactured by three different Brazilian companies, hereafter called A, B, C and D. Each of the geomembranes had a different thickness, which was: A = 2.0 mm, B = 1.90 mm, C = 1.70 mm and D = 0.80 mm, all with a smooth surface. For the study made by the TG and DSC analysis, pieces of diameter of each sample were around 3 mm.

Physical characterizations

Physical properties

Density measurements were [18] performed in isopropyl alcohol at 21 ± 0.1 °C, mass sample 1.0 g ± 0.1 g in apparatus that included an analytical balance with a 0.0001 g precision and an immersion vessel. A 25-mL pycnometer and a thermometer were used for solution standardization. The geomembrane thickness [19] was determined by observation, using a thickness gauge with 0.001 mm precision, applying a pressure force of 20 ± 0.2 kPa. The carbon black [20] content was determined by pyrolysis for about 1 ± 0.1 g of geomembrane in a muffle furnace at 605 ± 5 °C for 3 min in an aluminum dish.

Mechanical properties

Tensile [21], tear [22] and puncture resistance [23] tests were performed in an Emic Universal Testing Machine, Model DL 3000 with a 2-kN load cell and pneumatic grips. Speed rates of 50 and 300 mm min^{-1} for the tensile, tear and puncture tests were used.

Thermoanalytical methods

The thermogravimetric (TG) and differential thermal analysis (DTA) were performed at a SDT 2960 (TA Instruments, USA) with heating rates of 5, 10, 15 and 20 °C min^{-1} under nitrogen and synthetic air purge gases, with a flow of 100 mL min^{-1}. These polymers were evaluated in an α-alumina crucible. In addition, the kinetics study of these geomembranes was performed using the Flynn–Wall–Ozawa and Capela–Ribeiro methods, which are isoconversional methods [24–26].

To evaluate the behavior of these polymers by DSC analysis, the temperature range scanned was from 25 to 200 °C and from 200 to − 80 °C with a heating rate of 20 °C under nitrogen purge gas with a flow of 50 mL min^{-1}. The measurements were obtained from the DSC1 Star^{e} (Mettler Toledo) with a sample which had a diameter of around 2 mm and a weight variable.

The behavior of these polymers was tested on dynamic mechanic analysis (DMA) equipment using a DMA thermal analyzer (model Q800, TA Instruments). The experiments were performed in flexural mode. The dimensions of the samples were 64 mm × 12 mm × 3.0 mm. The experimental conditions were as follows: oscillation amplitude of 20 mm, frequency of 1 Hz, temperature range from −80 to 120 °C and a heating rate of 10 °C min^{-1}.

Results and discussion

Figure 1 shows the TG–DTG curves of the geomembrane samples in four heating rates under nitrogen purge gas. In the first evaluation, it can be observed that the thermal behavior of these materials is similar, i.e., they have a stability up to a high temperature and present only one stage of thermal decomposition. Along the same lines, the same occurs with the analyses seen in Fig. 2, where the geomembranes were analyzed under synthetic air as purge gas. As can be seen, under several heating rates, these samples have different thermal behaviors to one another. The main mass variations were obtained from DTG curves and are shown in Tables 1 and 2.

As can be seen in Fig. 2a, the analysis at 5 °C had a return in temperature from 407 to 402 °C, which was attributed to the combustion during the thermal

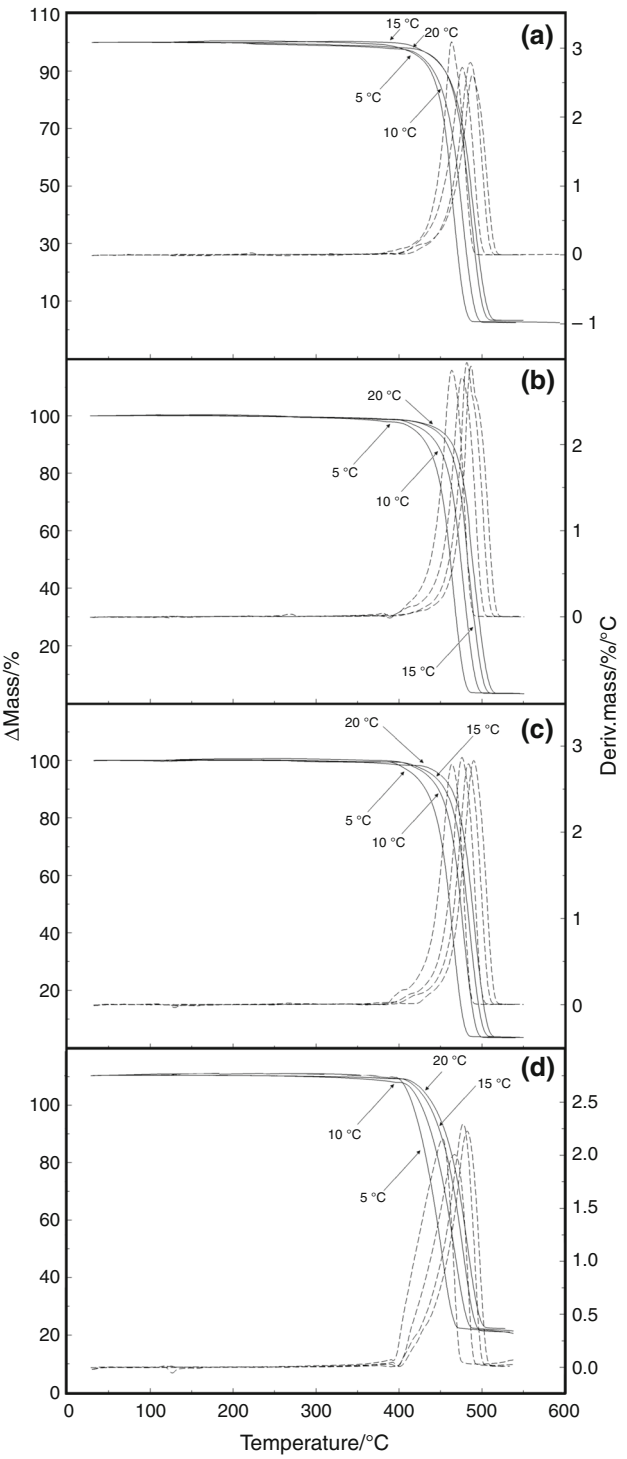

Fig. 1 TG–DTG curves of geomembranes with heating rates of 5, 10, 15 and 20 °C min^{-1} under nitrogen gas purge with flow of 100 mL min^{-1} in α-alumina crucible

decomposition. Additionally, there was an increase in temperature of the sample, which was greater than that of the furnace of the equipment. This same effect is seen for Sample 5B, but with a heating rate of 10 °C, where the

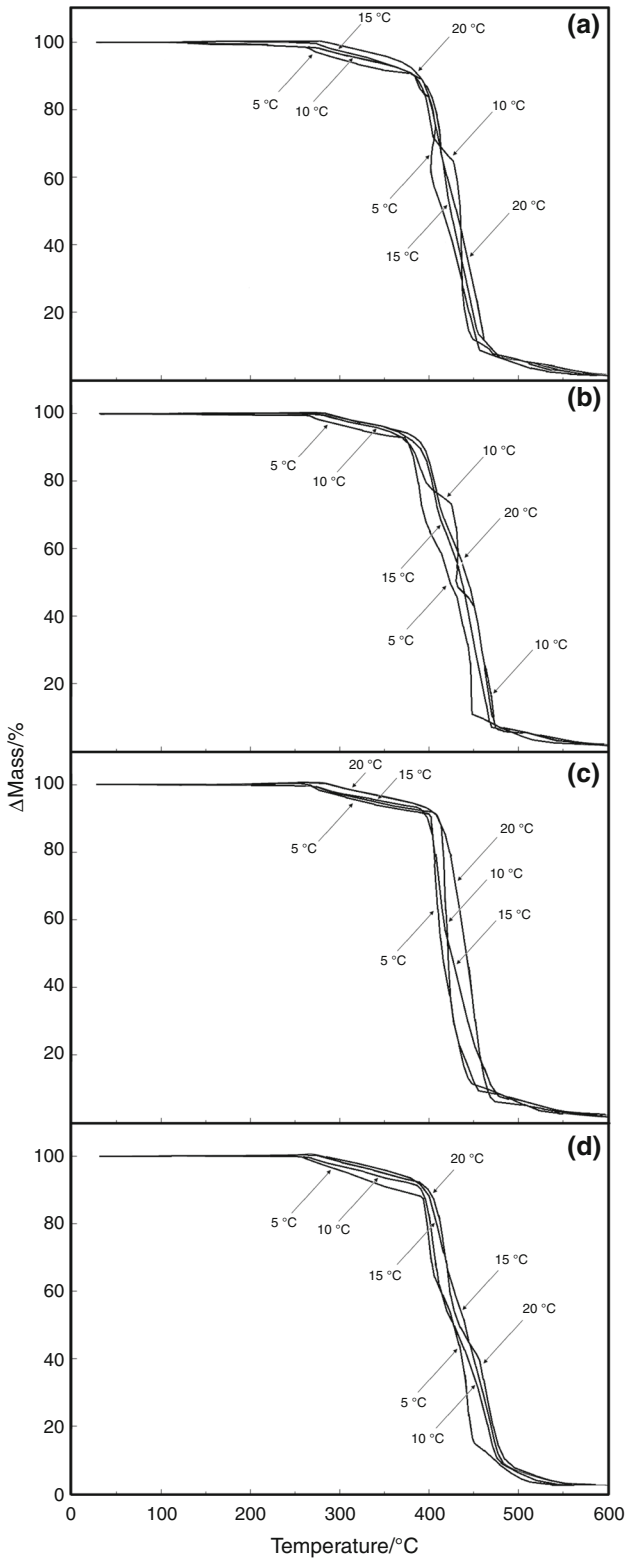

Fig. 2 TG–DTG curves of geomembranes with heating rates of 5, 10, 15 and 20 °C min^{-1} under synthetic air gas purge with flow of 100 mL min^{-1} in α-alumina crucible

temperature returns from 433 to 430 °C. The effect of the thermal decomposition can be seen in the TG–DTA curves (Fig. 3) with analyses performed on synthetic air purge gas at a heating rate of 10 °C min^{-1}. The first endothermic event seen between 90 and 150 °C refers to the melting point of the material, which is in agreement with the behavior seen in the DSC curves (Fig. 4). Between the melting point and the beginning of the first stage of thermal decomposition around 258 °C, there was no event recorded by the DTA curves. For Sample B, it can be observed that after starting the decomposition, the material had combustion, as observed for the analysis of 5 °C (Sample 2A), while for the other samples, there was no other combustion event.

Figure 4 shows the cooling and heating curves made by the DSC of the geomembranes. Initially, the samples were cooled from 25 to − 80 °C (curves not shown, because there are no thermal events). After this cooling, the material was heated from − 80 to 200 °C, except for Sample D, which was heated to 180 °C. During the melting point (peak temperture of 133 °C) it can be observed that the samples have overlapping reactions, which is more evident with the sample of 0.8 mm (Sample D). In the second heating (Fig. 4b), it can be seen that the melting point in DSC curves widens when compared to the first heating, which was attributed to the molecular relaxation. Figure 4d shows the cooling of the materials, where the exothermic reaction from 115 °C can be seen, which was attributed to the recrystallization of the material, while the weak exothermic events seen after peak recrystallization between − 3 and − 53° C are attributed to molecular rearrangement [27].

Kinetic behavior

The kinetic behavior was evaluated for each sample from the DTG curves, as can be seen in Fig. 1. For the analyses in purge gas in synthetic air, a kinetic study was not performed because the samples had different thermal behaviors from each other for each heating rate, as shown in Fig. 2.

The ranges used to study the kinetic behavior of the samples and the respective values of the activation energies of these materials are shown in Tables 3 and 4. The values obtained are very similar in behaviors for Samples A, B and C, but for Sample D (Fig. 5), there was an initial kinetic behavior different from the others. This fact was attributed to the thickness and, consequently, the mass of the sample, which is the smallest among them. However, it can be observed also at Fig. 5, that after the value of 0.15 in the conversion degree, the activation energy tends to remain at the same level, as was also observed for the other analyses.

Table 1 Temperature ranges (°C min^{-1}) and mass variations (%) seen at several stages of the TG curves of geomembranes under nitrogen purge gas

Geomembrane		5 °C	10 °C	15 °C	20 °C
Sample (A) 2.06 mm	Main temperature interval and mass variation	382–410 °C	399–417 °C	400–427 °C	397–431 °C
		1.31%	1.01%	1.43%	1.07%
		410–493 °C	417–503 °C	429–513 °C	431–518 °C
		94.38%	94.26%	93.64%	93.95%
Sample (B) 1.93 mm		397–492 °C	384–505 °C	410–510 °C	413–520 °C
		94.21%	94.88%	94.83%	− 94.88%
Sample (C) 1.67 mm		385–409 °C	392–421 °C	402–429 °C	421–439 °C
		2.67%	2.53%	2.41%	1.34%
		385–488 °C	421–501 °C	429–511 °C	421–513 °C
		92.94%	93.43%	− 93.05%	93.07%
Sample (D) 0.82 mm		393–483 °C	404–501 °C	409–508 °C	412–511 °C
		94.11%	93.22%	94.65%	93.59%

Table 2 Temperature ranges (°C min^{-1}) and mass variations (%) seen at several stages of the TG curves of geomembranes under synthetic air purge gas

Geomembrane		5 °C	10 °C	15 °C	20 °C
Sample (A) 2.06 mm	Main temperature interval and mass variation	259–380 °C	207–370 °C	267–385 °C	200–367 °C
		7.93%	7.96%	8.56%	6.10%
		380–395 °C	370–426 °C	385–482 °C	367–480 °C
		5.95%	27.56%	83.51%	87.30%
		395–458 °C	426–450 °C	–	–
		76.33 °C	52.50%	–	–
		458–600 °C	450–600 °C	482–600 °C	480–600 °C
		7.55%	10.95%	5.22%	5.44%
Sample (B) 1.93 mm		262–372 °C	264–359 °C	270–357 °C	274–368 °C
		6.89%	5.77%	4.87%	4.99%
		372–450 °C	359–420 °C	357–472 °C	368–475 °C
		82.36%	19.85%	88.59%	87.05%
		–	420–476 °C	–	–
		–	67.15%	–	–
		450–600 °C	476–600 °C	472–600 °C	475–600
		9.22%	5.73%	5.49%	4.60%
Sample (C) 1.67 mm		226–396 °C	263–402 °C	265–386 °C	274–393 °C
		8.69%	7.67%	6.08%	7.51%
		396–452 °C	402–454 °C	386–480 °C	393–477 °C
		80.79%	81.94%	86.11%	87.72%
		452–600 °C	454–600 °C	480–600 °C	477–600
		9.38%	7.90%	5.76%	4.45%
Sample (D) 0.82 mm		261–393 °C	263–386 °C	270–385 °C	271–387 °C
		11.59%	8.47%	7.88%	8.14%
		383–495 °C	379–520 °C	385–540 °C	387–540 °C
		84.33%	87.68%	88.20%	88.55%

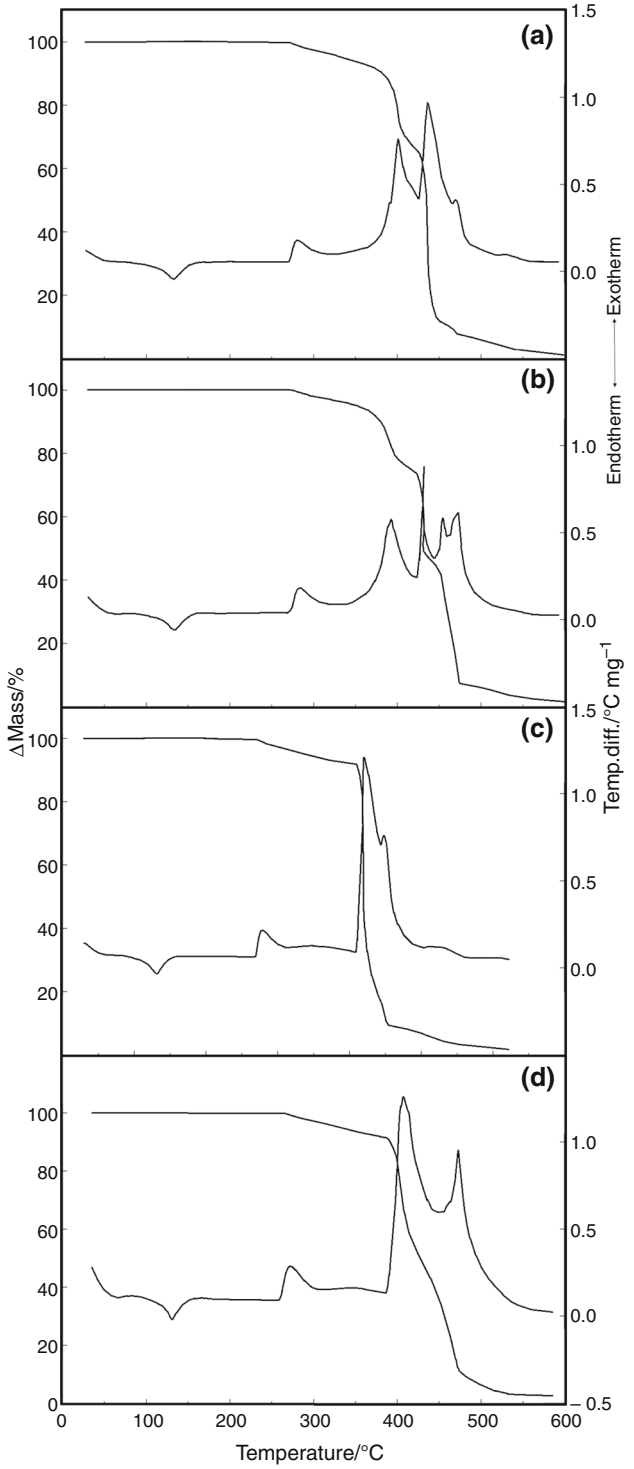

Fig. 3 TG–DTA curves of geomembranes with heating rate of 10 °C min^{-1} under synthetic air gas purge with flow of 100 mL min^{-1} in α-alumina crucible

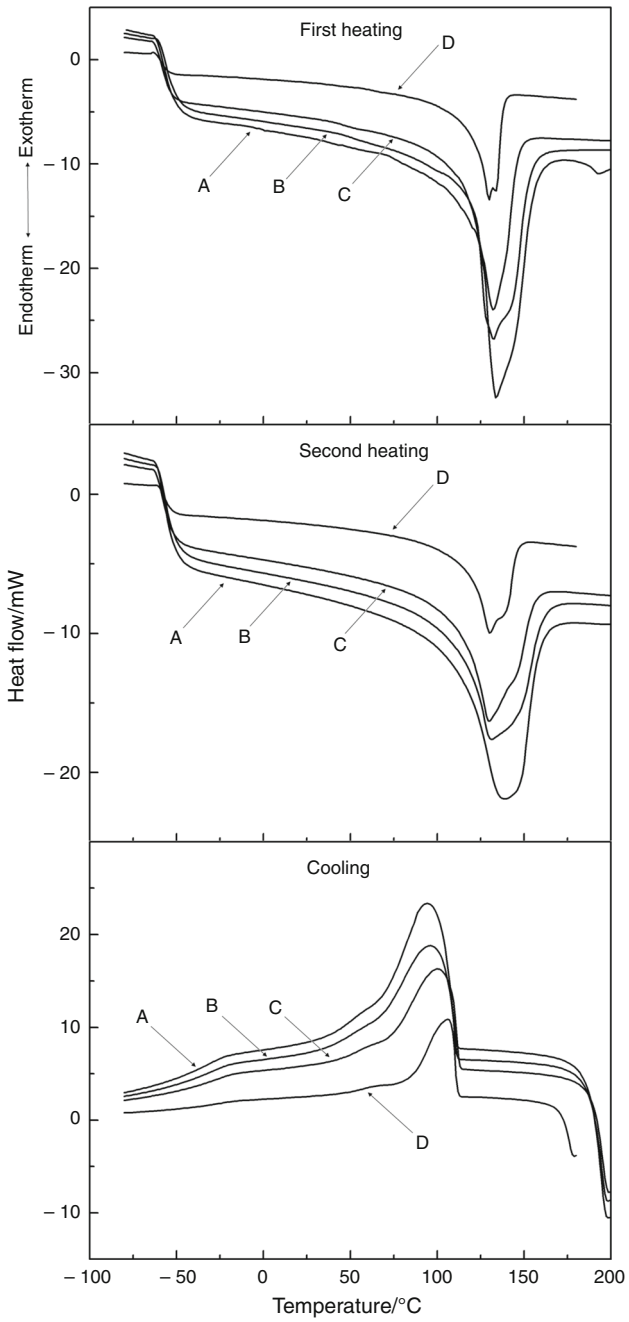

Fig. 4 DSC curves of geomembranes with heating rate of 20 °C min^{-1} under nitrogen gas purge with flow of 50 mL min^{-1} in aluminum crucible

Galwey indicates that kinetic parameters are dependent on factors attributed to the samples, such as geometry, particle distribution, heating rate of the sample, particle size, impurities and used atmosphere [28]. There are many studies in the literature on polymers, such as high-density polymers, which show different activation energy values. In addition, in studies found in the literature, it can be observed that there is no standard size and mass of the polymers analyzed in various published studies. Sinfrônio et al. report on thermal studies of HDPE decomposition in pellet samples with a mass of about 5 mg with several non-isothermal methods for kinetic evaluation. The results obtained by the Flynn–Wall–Ozawa method

Table 3 Temperature intervals (°C min^{-1}) of the main thermal decomposition of geomembranes utilized in the activation energy evaluation

Compound	5 °C	10 °C	15 °C	20 °C
(A)	400–495 °C	408–505 °C	424–514 °C	432–522 °C
(B)	398–492 °C	413–509 °C	428–515 °C	436–524 °C
(C)	381–492 °C	393–505 °C	402–511 °C	423–520 °C
(D)	395–478 °C	403–495 °C	406–505 °C	412–513 °C

Table 4 Activation energy values of geomembranes using the Flynn–Wall–Ozawa and Capela–Ribeiro methods

Samples	$E_a \pm$ VC/(kJ mol^{-1}) Capela and Ribeiro	$E_a \pm$ VC/(kJ mol^{-1}) Flynn–Wall–Ozawa
(A)	231.74 ± 0.05	254.51 ± 0.05
	0.97561	0.93719
(B)	217.44 ± 0.08	227.87 ± 0.09
	0.99961	0.99994
(C)	213.43 ± 0.11	227.35 ± 0.11
	0.99896	0.99953
(D)	177.56 ± 0.07	188.12 ± 0.06
	0.99661	0.99604

The data were obtained as an average arithmetic, and VC is the variation coefficient

showed that the activation energy increases from 162.49 to 230.48 kJ mol^{-1} and has an average value of 202.46 kJ mol^{-1}. This kinetic behavior is similar to the data obtained in this work for Samples 5A, 5B and 5C, but different from that obtained for Sample 5D [29]. Khedri and Elyasi reported the activation energy of HDPE (without indicating the source of the material used in the analysis) at the heating rates of 40, 45, 50 and 55 °C min^{-1} with sample masses around 13 mg by analyzing the non-isothermal condition. The activation energy obtained by these authors was among the interval of 70–100 kJ mol^{-1} [30]. Another evaluation of activation energy of the HDPE evaluated by the Flynn–Wall–Ozawa method was made by Avella et al. These authors compared the obtained values of compounds made with cellulose fibers and cellulose obtained from carton scraps. For pure HDPE, the activation energy values vary between 110 and 140 kJ mol^{-1}, while for the reinforced material, the values are higher than the pure polymer [31].

Physical methods

Table 5 shows the thickness values of the samples that are usually sold in Brazil, and as seen, compared to Table 6,

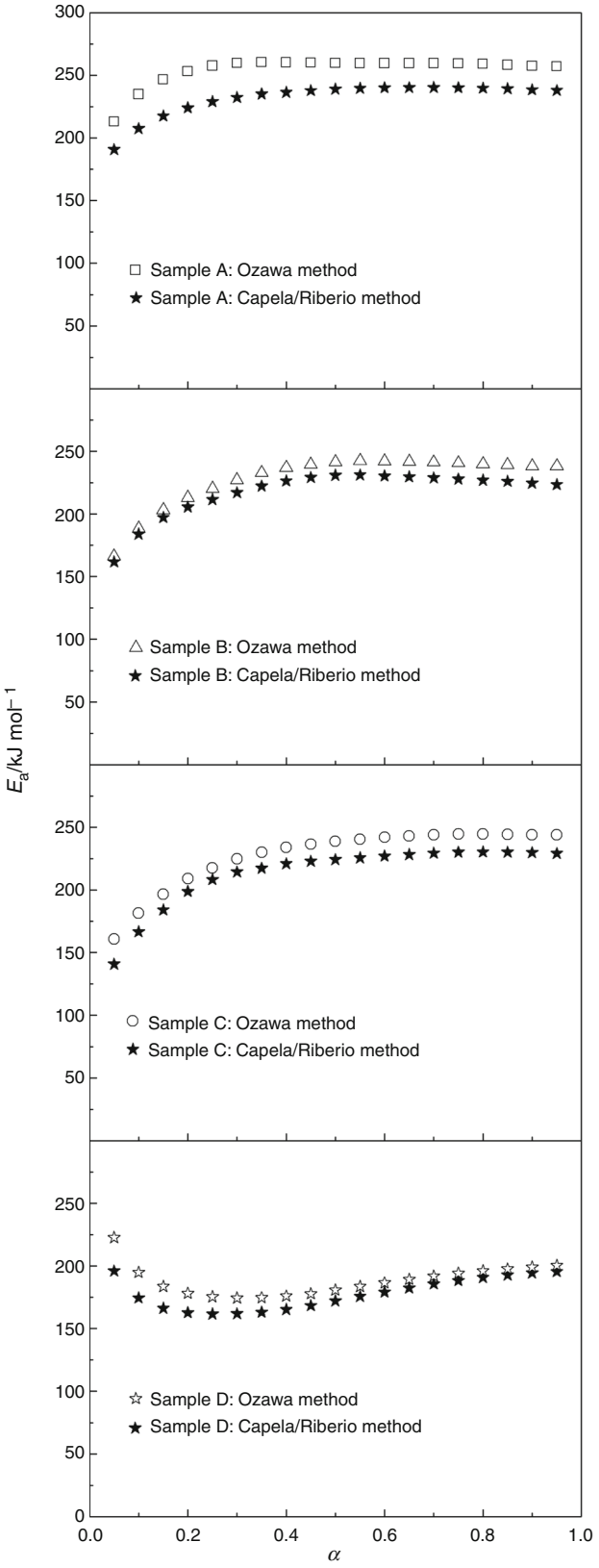

Fig. 5 Activation energy versus conversion degree (α) of geomembranes evaluated by the Flynn–Wall–Ozawa and Capela and Ribeiro methods

Table 5 Physical data obtained from geomembranes

Samples	Density/(g cm^{-3})	Thickness/ mm	Tens. yield resistance/ (kN m^{-1})	Tens. break resistance/ (kN m^{-1})	Tear resistance/N	Puncture resistance/N	CB
A	0.940	2.06	57.48	78.24	453.63	1171	2.21
	$\pm$ 6.1 $\times$ 10^{-4}	$\pm$ 0.0119	$\pm$ 0.0115	$\pm$ 0.1456	$\pm$ 0.0367	$\pm$ 0.0225	$\pm$ 0.0341
B	0.941	1.92	51.5	66.67	420.03	1093	2.54
	$\pm$ 0	$\pm$ 0.0039	$\pm$ 0.0412	$\pm$ 0.0633	$\pm$ 0.0498	$\pm$ 0.0126	$\pm$ 0.0409
C	0.940	1.67	36.42	52.81	309.26	916.83	2.86
	6.1 $\times$ 10^{-4}	0.0151	$\pm$ 0.0305	$\pm$ 0.1678	$\pm$ 0.0555	$\pm$ 0.0236	$\pm$ 0.0532
D	0.945	0.82	22.17	28.59	163.533	499.3	2.65
	$\pm$ 6.1 $\times$ 10^{-4}	$\pm$ 0.0281	$\pm$ 0.0763	$\pm$ 0.1090	$\pm$ 0.0384	$\pm$ 0.0349	$\pm$ 0.0548

Table 6 Physical, mechanical and chemical properties of HDPE geomembranes according to the standard specification by the Geosynthetic Research Institute [32]

Samples	Density/(g cm^{-3}) minimum	Thickness/mm minimum	Tens. yield resistance/ (kN m^{-1})	Tens. break resistance/ (kN m^{-1})	Tear resistance/N	Puncture resistance/N	CB
A	0.940	1.80	29	53	249	640	2–3
B	0.940	1.35	22	40	187	480	2–3
C	0.940	0.90	15	27	125	320	2–3
D	0.940	0.68	11	20	93	240	2–3

the results obtained showed that the measured values are in agreement with the criteria suggested by the Geosynthetic Research Institute [32]. However, as can also be seen in the values of Sample B, the thickness of 1.9 mm is the closest to the thickness suggested in Table 6, considering the thickness of 1.80 mm. The other values showed that the results are well above the reference values, demonstrating that the samples are reliable and can be used for proper use [33, 34].

Physical properties, such as thickness, identify the products and are related to mechanical properties, such as tensile, tear and puncture resistance. Reference information for well-established thermal property values such as DMA, TG–DTA and DSC is not usually used because they are considered to be expensive and have complex interpretation techniques [35, 36].

Dynamic mechanical analysis (DMA)

In the literature, the studies and presentation of the results carried out in the DMA focus on three main concepts: module storage, module loss and viscoelastic information of the material (tan δ) [37–39].

The DMA analysis under nitrogen purge gas in the range of 80–120 °C of the geomembranes is shown in Fig. 6, where it can be observed that the degree of stiffness shows a similar behavior among the samples. The variations of storage modulus normally indicate the degree of the crosslink in molecules of materials. Strictly speaking, at low temperatures, the polymer has a rigid behavior, and therefore, the storage modulus values will be high and when the temperature increases, the molecular vibrations also increase and then the storage modulus will decrease proportionally [37, 40]. For the sample with a thickness of 0.8 mm (Fig. 6a), the value of the module is smaller, which is expected, because a smaller thickness has a smaller storage modulus. Moreover, it can be observed that from 68 °C the storage module for all these samples present storage values very close to each other. In addition, if there were particles or reinforcing materials purposely added to these geomembranes in order to reinforce the material, the value of the modulus storage would be substantially larger. Some studies in the literature have shown the reinforcing effect on polymers, with clay, fibers and other polymers, causing an increase or decrease in the material stiffness, which will depend on the efficiency of the interaction between the reinforcement material and the polymer matrix [41–43].

The loss modulus (E'') is shown in Fig. 6b, where it can be observed that the 0.8-mm sample stands out from the other samples because the increase in E'' curves indicates that the sample could dissipate the energy vibration better in the form of heat than the other samples. From an industrial point of view, the amount of energy dissipated as

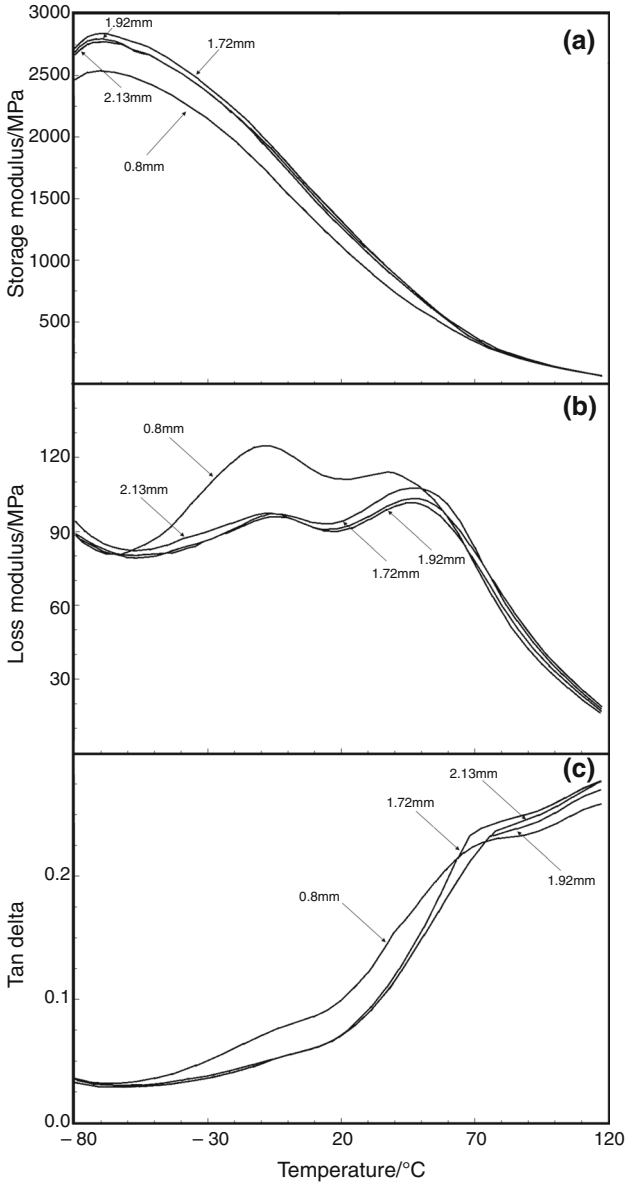

Fig. 6 DMA curves: **a** storage modulus, **b** loss modulus and **c** *Tan δ*

heat during deformation is important because the heat can be distributed into or out of the material itself [44].

Figure 6c shows the curves obtained from the tan δ versus temperature, which gives information on the contributions of the viscous and elastic components of viscoelastic materials. Since tan δ has a relationship between the loss and storage modules, the temperature ranges from − 60 to 20 °C and 20 to 70 °C as seen in Fig. 6a, b, which correspond to the events seen in Fig. 6c. Another important aspect is that normally, in polymeric materials, the value of tan δ increases when the value of the storage module (E') is decreased. As shown in Fig. 6c, when the temperature increases, the maximum value of tan δ also increases and this is attributed to the effect of molecular relaxation, i.e., with increasing molecular motility, energy is dissipated into the sample [45, 46]. In other words, the value of tan δ will be the maximum in the near values of the melting point of the HDPE, as seen for all samples, i.e., when the peak intensity of tan δ is higher, it indicates that the material responds viscously in detriment to elastic.

Conclusions

Four commercial geomembranes with various thicknesses were evaluated. The TG–DTA and DSC analyses showed the thermal behavior under different temperatures and purge gas conditions, leading to a thorough evaluation of these materials. The effect caused by using different purge gases on different heating rates (5, 10, 15 and 20 °C min^{-1}) can be observed. In addition, the different samples showed different thermogravimetric behaviors among them. The kinetic values showed that the sample of 0.8 mm had a different behavior during thermal decomposition. In DMA studies, the experimental results showed that there was a slight increase in the geomembrane of 0.8 mm, and no significant changes in the other samples. The temperatures of loss modulus and tan δ results showed two transitions in the viscoelastic region for these materials. The importance of these data is associated with the deformation effects of the geomembranes under a temperature effect and also in unhealthy environments caused by the pressure and heat that exist on the geomembranes, which are exerted by the deposition of residues in the geomembranes, associated with the presence of liquids and gases produced in landfills.

Concerning the mechanical properties, it can be observed that the density and black carbon data have compatible values between the samples, indicating that the materials were prepared in a similar way. Therefore, the values obtained for the tensile, tear and puncture tests are linked to the thickness of the material and show that commercial samples have much higher values than those recommended.

Acknowledgements The authors would like to thank the Geosynthetics Laboratory at the São Carlos School of Engineering (EESC) at the University of São Paulo (USP) for their support.

References

1. Fernandes MPM, Silva Filho LCP. Um modelo orientativo para a gestão municipal dos RCCs. Ambient Constr. 2017;17(2):21–38.
2. Prado Filho JF, Sobreira FG. Desempenho operacional e ambiental de unidades de reciclagem e disposição final de resíduos sólidos domésticos financiadas pelo ICMS ecológico de Minas Gerais. Eng Sanit Ambient. 2007;12:52–61.
3. Celere MS, Oliveira AS, Trevilato TMB, Segura-Muñoz SI. Metais presentes no chorume coletado no aterro sanitário de

Ribeirão Preto, São Paulo, Brasil, e sua relevância para saúde pública. Cad Saúde Pública. 2007;23(4):939–47.
4. Matos TFL, Schalch V. Composição dos resíduos poliméricos, pós-consumo, gerados no município de São Carlos, SP. Polímeros. 2007;17(4):346–51.
5. Koerner RM. Designing with geosynthetics. NJ: Prentice Hall; 1997.
6. Abdelaal FB, Rowe RK, Islam MZ. Effect of leachate composition on the long-term performance of a HDPE geomembrane. Geotext Geomembr. 2014;42:348–62.
7. Marielle GM, Durrieu C, Guenne A, Rouillac L, Diafi D, Nour I, Mazéas L, Nathalie TF, Farcas F. Impact of polyethylene and polypropylene geomembranes in sensitive aquatic environment. Ecotoxicol Environ Saf. 2018;148:884–91.
8. Nefso EK, Burns SE. Comparison of the equilibrium sorption of five organic compounds to HDPE, PP, and PVC geomembranes. Geotext Geomembr. 2007;25:360–5.
9. Touze-Foltz N, Bannour H, Barral C. Stoltz G A review of the performance of geosynthetics for environmental protection. Geotext Geomembr. 2016;44:656–72.
10. Aminabhavi TM, Naik HG. Chemical compatibility testing of geomembranes — sorption/desorption, diffusion, permeation and swelling phenomena. Geotext Geomembr. 1998;16:333–54.
11. Lavoie FL. Bueno BS Degradação de Membrana Impermeabilizante de Polietileno de Alta Densidade Usada em Tanques de Armazenamento de Vinhaça. Polímeros. 2013;23(5):690–5.
12. Costa CMLA, Lodi PC, Costa YDJ, Bueno BS. Avaliação de Recomendações Normativas sobre o Uso de Ensaios no Controle de Qualidade de Fabricação de Geossintéticos. Polím Ciên Tecnol. 2008;18(2):158–69.
13. Rajeshwari P. Kinetic analysis of the non-isothermal degradation of high-density polyethylene filled with multi-wall carbon nanotubes. J Therm Anal Calorim. 2016;123:1523–44.
14. Khedri S, Elyasi S. Determination of the heat of pyrolysis of HDPE via isothermal differential scanning calorimetry: A new approach for solid state reactions. J Therm Anal Calorim. 2018;131:1509–15.
15. Rowe RK. Ewais AMR Antioxidant depletion from five geomembranes of same resin but of different thicknesses immersed in leachate. Geotext Geomembr. 2014;42:540–54.
16. Aboulkas A, El Harfi K, El Bouadili A. Thermal degradation behaviors of polyethylene and polypropylene. Part I: pyrolysis kinetics and mechanisms. Energy Convers Manag. 2010;51:1363–9.
17. Al-Salem SM, Lettieri P. Kinetic study of high density polyethylene (HDPE) pyrolysis. Chem Eng Res Des. 2010;88:1599–606.
18. American standard test methods for density and specific gravity (relative density) of plastics by displacement D 792-00.
19. American standard test methods for measuring the nominal thickness of geosynthetics D 5199-06.
20. American standard test methods for determination of carbon black content in polyethylene compounds by the muffle-furnace technique D 4218-01.
21. American standard test methods for determining tensile properties of nonreinforced polyethylene and nonreinforced flexible polypropylene geomembranes D 6693-04.
22. American standard test methods for tear resistance (graves tear) of plastic film and sheeting D 1004-07.
23. American standard test methods for index puncture resistance of geotextiles, geomembranes, and related products D 4833-00.
24. Dias DS, Crespi MS, Ribeiro CA, Kobelnik M. Evaluation by thermogravimetry of the interaction of the poly(ethylene terephthalate) with oil-based paint. Eclét Quím. 2015;40:77.
25. Dias DS, Crespi MS, Kobelnik M, Ribeiro CA. Calorimetric and SEM studies of polymeric blends of PHB-PET. J Therm Anal Calorim. 2009;97:581–4.
26. Lima JS, Kobelnik M, Ribeiro CA, Capela JMV, Crespi MS. Kinetic study of crystallization of PHB in presence of hydroxy acids. J Therm Anal Calorim. 2009;97:525–8.
27. Trevino-Quintanilla CD, Krishnamoorti R, Bonilla-Rıos J. Flash DSC crystallization study of blown film grade bimodal high density polyethylene (HDPE) resins. Part 2. Non-isothermal Kinetics. J Polym Sci B Polym Phys. 2017;55:1822–7.
28. Galwey AK. Is the science of thermal analysis kinetics based on solid foundations? A literature appraisal. Thermochim Acta. 2004;413:139–83.
29. Khedri S, Elyasi S. Kinetic analysis for thermal cracking of HDPE: A new isoconversional Approach. Polym Degrad Stab. 2016;129:306–18.
30. Sinfrônio FSM, Santos JCO, Pereira LG, Souza AG, Conceição MM, Fernandes VJ Jr, Fonseca VM. Kinetic of thermal degradation of low-density and high-density polyethylene by non-isothermal thermogravimetry. J Therm Anal Calorim. 2005;79:393–9.
31. Avella M, Avolio R, Bonadies I, Carfagna C, Errico ME, Gentile G. Effect of compatibilization on thermal degradation kinetics of HDPE-based composites containing cellulose reinforcements. J Therm Anal Calorim. 2010;102:975–82.
32. Test methods, test properties and testing frequency for high density polyethylene (HDPE) smooth and textured geomembranes^{SM}. GRI—GM13 Standard Specification. Geosynthetic Institute. Accessed 6 Jan 2016, revision 14. http://www.geosynthetic-institute.org.
33. Abdelaal FB, Rowe RK. Effect of high temperatures on antioxidant depletion from different HDPE geomembranes. Geotext Geomembr. 2014;42:284–301.
34. Ewais AMR, Rowe RK, Asce F, Brachman RWI, Asce M, Arnepalli DN. Service Life of a High-Density Polyethylene Geomembrane under Simulated Landfill Conditions at 85 °C. J Geotech Geoenviron Eng. 2014;140(11):01–13.
35. Rollin A, Rigo J-M. Geomembranes identification and performance testing. London: Chapman & Hall; 1990.
36. Scheirs J. A guide to polymeric geomembranes: a practical approach. Wiley series in polymer science. London: Wiley; 2009.
37. Menard KP. Dynamic mechanical analysis: a practical introduction. New York: CRC Press; 1999.
38. Khonakdar HA, Morshedian J, Wagenknecht U, Jafari SH. An investigation of chemical crosslinking effect on properties of high density polyethylene. Polymer. 2003;44:4301–9.
39. Sewda K, Maiti SN. Dynamic mechanical properties of high density polyethylene and teak wood flour composites. Polym Bull. 2013;70:2657–74.
40. Lorandi NP, Cioffi MOH, Ornaghi H Jr. Análise Dinâmico-Mecânica de Materiais Compósitos Poliméricos. Sci Cum Ind. 2016;4(13):48–60.
41. Lofthouse MG, Burroughs P. Materials testing by dynamic mechanical analysis. J Therm Anal Calorim. 1978;13:439–53.
42. Gahleitner M, Grein C, Bernreitner K, Knogler B, Hebesberger E. The use of DMTA for predicting standard mechanical properties of developmental polyolefins. J Therm Anal Calorim. 2009;98:623–8.

43. Yang HS. Thermal and dynamic mechanical thermal analysis of lignocellulosic material-filled polyethylene bio-composites. J Therm Anal Calorim. 2017;130:1345–55.
44. Kinloch AJ, Young RJ. Fracture behaviour of polymers. Dordrecht: Springer; 1995.
45. Khonakdar HA, Wagenkecht U, Jafari SH, Hassler R, Eslami H. Dynamic Mechanical Properties and Morphology of Polyethylene/Ethylene Vinyl Acetate Copolymer Blends. Adv Polym Tech. 2004;23:307–15.
46. Molefi JA, Luyt AS, Krupa I. Comparison of the influence of copper micro- and nano-particles on the mechanical properties of polyethylene/copper composites. J Mater Sci. 2010;45:82–8.